

LEVEL #

T2

AD A089404

Figures of Merit for Mirror Materials

E. G. WOLFF
Materials Sciences Laboratory
Laboratory Operations
The Aerospace Corporation
El Segundo, Calif. 90245

10 July 1980

Interim Report

APPROVED FOR PUBLIC RELEASE;
DISTRIBUTION UNLIMITED

DTIC
ELECTE
SEP 23 1980

Sponsored by

DEFENSE ADVANCED RESEARCH PROJECTS AGENCY (DoD)
DARPA Order No. 3646
Monitored by SD under Contract No. F04701-79-C-0080

SPACE DIVISION
AIR FORCE SYSTEMS COMMAND
Los Angeles Air Force Station
P.O. Box 92960, Worldway Postal Center
Los Angeles, Calif. 90009



THE AEROSPACE CORPORATION

THE VIEWS AND CONCLUSIONS CONTAINED IN THIS DOCUMENT ARE THOSE OF THE AUTHOR AND SHOULD NOT BE INTERPRETED AS NECESSARILY REPRESENTING THE OFFICIAL POLICIES, EITHER EXPRESSED OR IMPLIED, OF THE DEFENSE ADVANCED RESEARCH PROJECTS AGENCY OR THE U.S. GOVERNMENT.

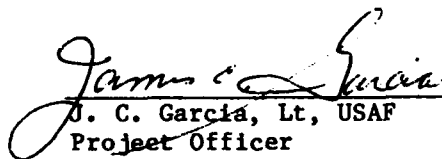
80 9 22 241

DDC FILE COPY

This interim report was submitted by The Aerospace Corporation, El Segundo, CA 90245, under Contract No. F04701-79-C-0080 with the Space Division, Deputy for Technology, P.O. Box 92960, Worldway Postal Center, Los Angeles, CA 90009. It was reviewed and approved for The Aerospace Corporation by W. C. Riley, Director, Materials Sciences Laboratory. Lieutenant J. C. Garcia, SD/YLXT, was the project officer for Technology. Dr. H. Allan Pike is the Program Director for the DARPA Washington Office. This research was supported by the Defense Advanced Research Projects Agency of the Department of Defense.


This report has been reviewed by the Public Affairs Office (PAS) and is releasable to the National Technical Information Service (NTIS). At NTIS, it will be available to the general public, including foreign nations.

This technical report has been reviewed and is approved for publication. Publication of this report does not constitute Air Force approval of the report's findings or conclusions. It is published only for the exchange and stimulation of ideas.


J. C. Garcia, Lt, USAF
Project Officer


Joseph T. Cox, Lt Col., USAF
Chief, Advanced Technology Division

FOR THE COMMANDER


Burton H. Holaday
Director of Technology Plans and
Analysis
Deputy for Technology

UNCLASSIFIED

SECURITY CLASSIFICATION OF THIS PAGE (When Data Entered)

REPORT DOCUMENTATION PAGE		READ INSTRUCTIONS BEFORE COMPLETING FORM
1. REPORT NUMBER SD-TR-80-35	2. GOVT ACCESSION NO. AD-A089404	3. RECIPIENT'S CATALOG NUMBER
4. TITLE (and Subtitle) FIGURES OF MERIT FOR MIRROR MATERIALS	5. TYPE OF REPORT & PERIOD COVERED Interim rept.	6. PERFORMING ORG. REPORT NUMBER TR-0080(5762-02)-1
7. AUTHOR(s) Ernest G. Wolff	8. CONTRACT OR GRANT NUMBER(s) F04701-79-C-0080	9. PROGRAM ELEMENT, PROJECT, TASK AREA & WORK UNIT NUMBERS N/DARPA Order-3646
10. PERFORMING ORGANIZATION NAME AND ADDRESS The Aerospace Corporation El Segundo, Calif. 90245	11. CONTROLLING OFFICE NAME AND ADDRESS Defense Advanced Research Projects Agency 1400 Wilson Blvd. Arlington, VA 22209	12. REPORT DATE 10 July 1980
13. MONITORING AGENCY NAME & ADDRESS (if different from Controlling Office) Space Division Air Force Systems Command Los Angeles, CA 90009	14. NUMBER OF PAGES 39	15. SECURITY CLASS. (of this report) Unclassified
16. DISTRIBUTION STATEMENT (of this Report) Approved for public release; distribution unlimited		
17. DISTRIBUTION STATEMENT (of the abstract entered in Block 20, if different from Report)		
18. SUPPLEMENTARY NOTES		
19. KEY WORDS (Continue on reverse side if necessary and identify by block number) Thermal and mechanical stability Mirror distortion Mechanical loading effects Thermal loading effects		
20. ABSTRACT (Continue on reverse side if necessary and identify by block number) Potential mechanisms that result in excessive wavefront distortions by large mirrors are reviewed, with the objective of defining the mirror substrate material property requirements in each case. A generalized figure of merit is found to require maximal thermal conductivity, elastic modulus, strength, melting point, and dimensional stability. The thermal expansion coefficients and their variability must be minimized. The analyses can be used to optimize mirror design and materials for a wide range of mechanical and thermal loading conditions.		

DD FORM 1473
(FACSIMILE)

UNCLASSIFIED

SECURITY CLASSIFICATION OF THIS PAGE (When Data Entered)

PREFACE

The author is grateful to R. J. Champetier and E. W. Silvertooth for helpful comments and suggestions.

Accession For	
Dist	<input checked="checked" type="checkbox"/>
Dist	<input type="checkbox"/>
Dist	<input type="checkbox"/>
Dist	<input type="checkbox"/>
For	
Distribution/	
Availability Codes	
Dist	Avail and/or special
A	

CONTENTS

PREFACE.....	1
I. INTRODUCTION.....	5
II. THEORY.....	9
III. MIRROR FAILURE CRITERIA.....	13
A. Mechanical Loading Effects.....	13
B. Thermal Loading Effects.....	23
IV. FIGURES OF MERIT.....	33
REFERENCES.....	35
SYMBOLS	41

I. INTRODUCTION

Large space mirrors were analyzed¹ with the objective of comparing the ability of materials to minimize static, thermal, and dynamic load-induced deflections. The behavior of the mirror was associated with the central deflection or sag δ when it was simply supported along its periphery. Geometry, loading conditions, and bulk material properties jointly affected the distortion of a mirror. This analysis generalizes the initial approach to cover most potential failure modes of large optical and laser mirrors. Material properties are examined as they relate to the performance of an optical train and as they combine into figures of merit for selected failure criteria. The objective is to optimize mirror substrate and support materials to permit more stringent loading conditions, greater geometrical flexibility, and improved performance in terms of thermal and mechanical stability. In addition, these figures of merit should aid in the determination of the importance of advances in material properties.

The scope of this study is limited to factors responsible for quality degradation in high-power laser systems that are attributable to mirrors, principally phase distortions and power absorption. The range of power optics includes electromagnetic pulse damage and overall power handling abilities.² Performance of an optical train is influenced by many factors, such as misalignments, beam obscuration, laser characteristics, and interactions with active positioning devices.³ Although we attempt, in this report, to deal with all factors that influence mission requirements, mirrors in a gaseous environment are not considered. Boundary-layer and thermal-blooming effects may occur in such an environment. Related topics such as thermal mechanisms in thin films and scattering as a measure of laser damage assessment are also considered peripheral to the choice of mirror substrate and support materials.

Many material figures of merit have been proposed in connection with mirror substrates (see, for example, the list in Table I). This background material was used to make the present study as comprehensive as possible; a major objective was to combine the most relevant material parameters for comprehensive figures of merit.

Table I. Some Figures of Merit for Mirror Materials

$\alpha/E^{1/2}$	Hexagonal distortion factor
α/E	Thermal-gradient effects
α/K	Linear-temperature gradients
$\alpha/\rho C_p$	Speed of response to transient thermal inputs
α/KE	Despace figure of merit for a telescope
$\alpha(1+\nu)/\rho C_p$	Localized transient distortion
$\alpha(1+\nu)$	Distortion of substrate if poorly cooled, pulsed
$\alpha(1+\nu)/K$	Well-cooled, repeated pulse deformations
$\alpha/\sqrt{K \rho C_p}$	Time to reach average temperature
$\alpha E^{1/3}/K$	General distortion factor
$\alpha E/K$	Actuator-load requirements
$\alpha E/\sigma_{MYS}$	Thermal-fatigue resistance
$\alpha E(1-\nu)$	Thermal-stress limit
$\alpha E \sigma_U(1-\nu)$	Thermal-fatigue resistance
$\alpha \rho/K \sigma_{MYS} E$	General figure of merit for mirror substrates
$\sigma \rho C_p/K \sigma_{MYS} E$	General thermal deformations
E_c	Short-column buckling analysis
E/ρ	Self-weight, mirror support points
$E/\rho(1-\nu^2)$	Dynamic loading, constant thickness
$E/\rho \nu$	Sag due to self-weight
$E/(1/3-\nu^2)$	Buckling damage
$E/\rho^3(1-\nu^2)$	Dynamic loading constant mass/area
$E \sigma_{MYS}/\rho$	Thermal soak deformation on weight basis
$E \sigma_{MYS}/\rho$	Long-term dimensional stability
$(K \rho C_p)^{1/2}/(T_m - T_o)$	Melt damage from pulsed lasers
$G/(1-\nu^2)$	Shear deformations of supports
$K/\rho C_p$	Thermal diffusivity
$K \rho C_p$	Transient deformation (cw)

Table I. Some Figures of Merit for Mirror Materials (Continued)

$K\rho L_E$	Vaporization damage
$K\rho C_p(T_m - T_o)$	Maximum energy density from pulsed lasers
σ_{U^0}	Crack sensitivity

II. THEORY

Material figures of merit are derived on the basis of the ability of a mirror's properties to minimize the deformation of a wavefront in the presence of changing mechanical or thermal loading conditions. An rms phase aberration $\Delta\phi$ is added to a wavefront when the mirror exhibits an rms distortion in the optical path length $\Delta\ell$ in the beam path direction, or

$$\Delta\phi = \frac{2\pi}{\lambda} \Delta\ell \quad (1)$$

The far-field intensity I can be computed for small aberrations, if we assume that the baseline intensity I_0 is proportional to the total power level of the beam. As indicated by Born and Wolf,⁴ the intensity at the focus, or center of a Gaussian reference sphere of the nonaberrated beam is

$$\frac{I}{I_0} = \frac{1}{\pi^2} \left| \int_0^{\ell} \int_0^{2\pi} e^{i\Delta\phi} \rho d\rho d\theta \right|^2 \quad (2)$$

where the integration is over the aperture of radius ρ and polar angle θ . The Strehl approximation⁴⁻⁶ is

$$\frac{I}{I_0} = 1 - (\Delta\phi)^2 = 1 - \frac{2\pi}{\lambda}^2 (\Delta\ell)^2 \quad (3)$$

Clearly, $\Delta\phi$ must be <1 radian ($\lambda/2\pi$), otherwise $I \rightarrow 0$. Winsor⁶ shows that the limit of validity is generally

$$\Delta\phi < 0.55 \text{ rad} < \lambda/11.5 \quad (4)$$

The Marechal criterion ($\Delta\phi = 0.447$) is convenient to use for describing the required performance of an optical train. Distortions are commonly divided into figuring errors σ_f , and changes in optical figures either correlated or uncorrelated with the beam intensity profile. For mirrors, many distortions are linearly power dependent, but others may be related to factors such as mechanical loading changes. This distinction is important when the various distortions are summed to calculate a total aberration in the optical train.⁶ The optical path length distortion Δl for a single mirror is

$$\Delta l = 2 \sqrt{\sigma_f^2 + \bar{\delta}_{\text{rms}}^2 (I_o) + \bar{\delta}_{\text{rms}}^2} \quad (5)$$

where

$$\bar{\delta}_{\text{rms}}^2 = \frac{1}{2\pi a^2} \int_0^{2\pi} \int_0^a \delta^2 r dr d\theta \quad (6)$$

and δ is the axial (z direction) displacement of the surface; δ is a function of material parameters: time, geometry, and power density. The factor of 2 in Eq. (5) represents the fact that the optical path length decreases by twice the axial movement of the mirror surface. Equations (3) and (5) combined with the Marechal criterion indicate that

$$\sigma_f^2 + \bar{\delta}_{\text{rms}}^2 = \lambda^2/80\pi^2 \quad (7)$$

where $\bar{\delta}_{rms}^2$ is either the power correlated or uncorrelated surface distortion. It is seen that σ_f must be $\leq \lambda/28$, which is also the maximum value that can be tolerated for distortion. If λ is $10.6 \mu\text{m}$, $\bar{\delta}_{rms}$ must be $\leq 0.377 \mu\text{m}$ or $\leq 15 \mu\text{in.}$ This is the order of magnitude of maximum allowable displacements.

Material parameter contributions to δ must, therefore, be minimized. Their combinations will serve as useful figures of merit for maximizing the far-field intensity I [Eq. (3)] or the permissible power density I_0 , when $\delta_{rms} = f(I_0, t)$.

Alternative approaches include the criterion of a change in the depth of focus of a mirror.⁷ The change in radius of curvature is then of interest, rather than only local or integrated axial deflections [Eq. (6)]. However, such an analysis yields very similar figures of merit and is not as comprehensive. Alternatives to surface distortion, such as temperature-dependent damage failure modes,⁸ are discussed briefly in this report. Sparks⁹ defined figures of merit for laser windows in terms of an angle through which normally incident light is bent. A comparable failure mode for mirrors might be excessive scattering or changes in absorptance. These are normally attributed to surface effects and not to substrate material properties. A possible exception might exist if the angular spread from a reflected ray is regarded as a function of surface dimples, or bumps¹⁰ whose appearance may be caused by nonuniform thermo-mechanical effects and whose magnitude depends on substrate material parameters.

III. MIRROR FAILURE CRITERIA

Table II lists potential failure modes in mirrors that depend on the substrate and support structure materials. Expected application areas for spacecraft are listed next, followed by the relevant material figures of merit. The failure modes are divided into two categories: mechanical effects and thermal effects, including laser damage effects. The common failure criteria are excessive surface displacement and unacceptable surface degradation, e.g., melting. The derivation of figures of merit is described in this section.

A. MECHANICAL LOADING EFFECTS

Mathematical models generally assume a thin shell for the mirror. Analysis becomes much more complex if $2a/h < 3$, at which point >15% error is probable.⁵ Elastic distortion as a function of stresses (and temperature variations) can be calculated by methods of dynamic relaxation.¹¹ In this approach, the material parameters involved using Hooke's law are E, G, ν (and α). Effects of nonsymmetric stress (or temperature) distributions can be handled with computer programs based on such analyses.

1. SELF-WEIGHT CONSIDERATIONS

The sag resulting from self-weight (or steady-state accelerations) is described in Ref. 1 as

$$\delta = \frac{3}{4} a^4 \frac{(1 - \nu^2)\rho^3}{E_{11}} \frac{I_s}{I} \frac{g}{m^2} \quad (8)$$

I_s and I are, respectively, the moments of inertia of a solid cross section and of a built-up section of the same area. This results in an $E_{11}(1 - \nu^2)^{-1}\rho^{-3}$ material figure of merit. A slightly different approach¹² describes the sag as

Table II. Potential Mirror Failure Modes

Mechanical Loading Effects			
	<u>Occurrence</u>	<u>Material Figures of Merit</u>	<u>References</u>
Self weight	Gravity and steady state accelerations	$E\rho^{-3}(1-\nu^2)^{-1}$ $E/\rho\nu$	1, 12
Dynamic loading	Launch vibration deployment	$E\rho^{-3}(1-\nu^2)^{-1}$	1
Stress waves	Laser/EMP	α, σ_{MYS}	13, 14, 60
Actuator-induced stresses	Active figure control positioning	$\sigma_{MYS}, E/\rho$	16-19, 21
Support stress	Fastener internal cooling	$\nu, \sigma_{MYS}, E/\rho, G$	1, 22, 23
Buckling of supports	Launch deployment	G, E^C	1, 22, 25, 26
Temporal stability	Fabrication, residual stresses, storage	$E/\rho, \sigma_{MYS}$	1, 24, 27-30, 53-56
Coating effects	Fabrication	E	2, 47, 57

Table II. Potential Mirror Failure Modes (Continued)

Thermal Effects			
<u>Steady-State Deflections</u>	<u>Occurrence</u>	<u>Figure of Merit</u>	<u>References</u>
Radiation coupled to backup, curved	Incident flux	k_L/α_{11}	1
Radiation coupled to backup, flat	Incident flux	k_L/α_{11}	1
$\Delta T_b = \Delta T_g$, curved	Change to operating T	$\bar{\alpha}_{11}$	7
$\Delta T_b = \Delta T_g$, flat	Out-of-plane growth	$\bar{\alpha}_{11}$	34
Linear gradients, curved	Uniform flux	k_L/α_{11}	34
Linear gradients, flat	Uniform flux	k_L/α_{11}	1
Variations in CTE	Compositional variations in substrate	$(1 + \nu)\Delta\alpha/\rho C_p$	1, 35, 36
<u>Transient Deflections</u>			
Short-time thermal effects	Pulsed Lasers melting, vaporization	$\sqrt{\rho C k} \rho L_p^k \rho L_e^k$	8, 32, 37, 58
Long-time distortions	CW laser	$\rho C_p \alpha$	5, 8, 35, 36, 43
<u>Thermally Induced Failure</u>			
Thermal cracking	Nonuniform heating	$k/\alpha E$	11, 36
Thermal fatigue	Pulsed lasers Thermal cycling	$E\alpha(1-\nu)^{-1}(\rho C k)^{-1/2}$	58
Miscellaneous damage mechanisms	Impurity effects	$k\rho C_p$	19, 32, 46

$$\delta = -\frac{g\rho v}{2E} a^2 - \frac{1}{8} \frac{(2\rho gh)}{D} a^2 \left[\frac{1}{8} \left(\frac{5+v}{1+v} \right) a^2 + \frac{1}{5} \left(\frac{8+v+v^2}{1+v^2} \right) \right] h^2 \quad (9)$$

which suggests a figure of merit of $E/\rho v$ to be maximized.

2. DYNAMIC LOADING

The corresponding deflection is given in Ref. 1 as

$$\delta = 0.22 \frac{a^3}{m^3} \frac{\rho^3(1-v^2)}{E_{11}} \left(\frac{I_s}{I} \right) \frac{\bar{F}}{\xi} \quad (10)$$

where the relevant material figure of merit is $E(1-v^2)^{-1} \rho^{-3}$, the same as in the static loading case. In this case, δ is the peak resonant mirror deflection and \bar{F} the amplitude of a disturbing function. The latter may be a random or sinusoidal vibration, mechanical shock, or spinning centrifugal load.

3. STRESS-WAVE EFFECTS FROM LASERS

Laser-induced stress waves in an elastic medium follow a wave equation of the form:¹³

$$\frac{\partial^2 u}{\partial z^2} - \frac{\rho}{E} \frac{\partial^2 u}{\partial t^2} + \frac{(v r_G)^2}{E} \frac{\partial^4 u}{\partial z^2 \partial t^2} = 0 \quad (11)$$

where u is the displacement, which varies with z and t . When heating can be considered instantaneous,

$$\left(\frac{\partial u}{\partial z} \right)_{t=0} = -\alpha T_{\max} \exp(-\beta z) \quad (12)$$

and the strain amplitude is proportional to αT_{\max} , which is in turn proportional to the deposited energy. The CTE (or α) is the principal material figure of merit here. The displacement may, if excessive, cause plastic deformation, in which case the microyield strength (MYS) is important. It is well known that pulsed lasers can cause microstructural changes.¹⁴ Required stress-wave amplitudes are on the order of 1 to 10 GPa. A common location for such failure is at an interface where one material is transparent to the laser beam.

4. ACTIVATOR-INDUCED DISTORTIONS

Adaptive optics is a complex subject. In this report, we consider only formulas that relate actuator parameters (force, position, etc.) to mirror substrate material properties. Wavefront information is applied to an actuator at some position behind the first surface mirror plate. Correction of the major figure error usually results in a new mode of distortion, which is also affected by neighboring actuators (influence function).¹⁵

The deflection y of a uniformly loaded beam with a concentrated corrective load P is¹⁶

$$y = \frac{px}{24EI}(L^3 - 2Lx^2 + x^3) - \frac{Px}{12EI}x^2 - \frac{3L^2}{4} \quad (13)$$

where $0 < x < L/2$, and p is the uniformly distributed load. Therefore, for a zero deflection $y = 0$, and $P = (5/8) pL$, which results in removal of 97% of the rms error (for the first three vibrational modes). The larger E , the smaller the deflections involved (for fixed loads). The criterion for actuator spacing is

$$\ell = \frac{\sqrt{Rh}}{\sqrt[4]{12(1-\nu^2)}} \quad (14)$$

which, except for the Poisson's ratio, is essentially independent of material properties. This indicates that to minimize the number of actuators, and thus the cost, the thickness h should be large, and in a weight-constrained design the density should be low.

In addition to E , ρ , and ν , the MYS is likely to be important in areas where the actuator forces are applied to correct for the mirror figure errors. The flexural rigidity is of primary importance when moments, rather than unidirectional translations, are used.¹⁷ This involves the $E/(1 - \nu^2)$ term.

Hogge¹⁸ described zonal (assumed above) versus modal corrector methodologies. The modal approach involves deformation of the entire mirror surface into a set of specific functions (e.g., Zernicke polynomials) to correct for aberrations caused by vibrations or jitter. This approach probably will also be affected by E , ν , and ρ but in different combinations than for the zonal methods. Actuators normally handle distortions at rates of <100 Hz. Resonant frequencies are proportional to $(EI/\rho)^{1/2}$, but distortions are generally $\sim \rho/E$. Therefore, E/ρ should be high to keep resonances above 100 Hz, but if it is too high, the forces required by actuators may become excessive (if the aberrations are large). Large aberrations tend to reduce mirror frequency response to even lower values (e.g., 5 Hz, Ref. 20). A breakdown of the required elastic constants involved for piezoelectric control is given by Adelman.²¹

5. SUPPORT STRESS

Deformations can occur in the mirror support structure for reasons unrelated to mirror substrate behavior. In the absence of correction devices such as actuators, these deformations may affect the figure and thus mirror performance. Even with actuators, these deformations should be minimal to simplify the role of the active controls. Spacecraft attitude changes induce stresses into the mirror support system from temperature changes as in the Large Space Telescope or during deployment (slew loads) and course adjustments. In high energy laser systems, when the pulsewidth is sufficiently long for steady-state heat transfer, a quasi-cw situation results where thermal distortions of

the support column and backup structure help determine mirror surface distortions. Local mirror surface distortions may also be induced by the presence of cooling channels for high power mirrors. Deflections caused by stress changes in supports are generally proportional to E/D , where D is the flexural rigidity.

$$D = \frac{Eh^2}{12(1 + \nu)^2} \text{ (solid plate), or } D = \frac{t(h + t)^2 E}{2(1 + \nu^2)} \text{ (sandwich) (15)}$$

where t is the thickness of the upper and lower plates. A low Poisson's ratio is desirable.

Supports may also be subject to shear deformations and microplastic deformation, which all cause mirror distortion. The shear component of the deformation in a mirror substrate is expected to be small for large span-to-thickness ratios of solid plates but will be significant in any sandwich-type cross section. The influence of shear forces on the total deflection may equal or exceed that of pure bending behavior of a mirror blank.²² Selke found that for moderately thick plates with thickness-to-diameter ratios of >0.1 , shear effects can contribute significantly to the total deflection.²³ Large optics, i.e., with low flux environments, are not likely to exceed the 0.1 ratio, but, if thick foam supports are used, there may be a problem. Important material parameters include the shear modulus and the flexural rigidity [which contains the $E/(1 - \nu^2)$ parameter]. The effective shear modulus will depend on core construction as much as on materials used, e.g., rib thickness, pore size, and foam. The core cell geometry and bonding techniques should also be considered when efforts are made to maximize the effective shear modulus to minimize deflections, since it may be undesirable to increase G by increasing the core density.

The microyield strength must be high for the material to resist small permanent deformations caused by short-term loads. It is doubtful if any material is perfectly elastic at arbitrary small distortion levels. Stress and plastic strain behavior of mirror substrate materials are discussed in

Ref. 24. The gravity-release effect on support systems may result in anelastic effects on many low-expansion materials. Recovery rates from temporary loads are important for the estimation of residual mirror figures. A possible guideline is that materials exhibit similar creep strains at equal percentage of their MYS values. Microstrain behavior is also proportional to shear moduli.¹⁴

6. BUCKLING OF SUPPORTS

A common lightweight mirror structure consists of two thin plates connected by a low-density core structure. The cross section of this core may be a foam, a grid, or periodic I-beam supports. Ayer¹ and Barnes²² have presented equations for the flexural rigidity D and central deflections as a function of rib thickness t , rib height h , and plate thickness th . The advantages in reducing t to obtain high values of I/I_s are ultimately negated by the susceptibility to compressive buckling under polishing or launch loads. If the I cross section is close to orthogonal (small vertical deviation), the I-beam web can be regarded as a long, simply supported plate. The critical load for buckling P_{cr} is conservatively estimated at

$$P_{cr}(lb/in) = \left(\frac{E}{1 - \nu^2} \right) \frac{\pi^2}{12} \frac{t^3}{d^2} \quad (16)$$

where the first term contains all the material parameters. The larger $E/(1 - \nu^2)$, the smaller the permissible web thickness, if we assume P_{cr} is fixed at the MYS or proportional limit or similar criterion. The maximum permissible I/I_s can then be calculated; for example,

$$\frac{I}{I_s} = \eta^3 - (1 - t) \left[\eta - \frac{(1 - \eta t)}{(1 - t)} \right]^3 \quad (17)$$

where η is approximately equal to the ratio of h to the height of a solid core of the same cross-sectional area.

Light weighting as such does not necessarily reduce deflections, but it improves bending resistance and E/ρ of mirror structures in general. Greszczuk reviewed theories of microbuckling of unidirectional composites.²⁵ In general, extensional and shear, elastic and inelastic buckling modes must be considered. The shear modulus of the matrix and elastic modulus of the fibers are major material parameters to be maximized. Geometry is as important as material parameters. Elastic buckling stresses also vary, depending on whether there are free edges (e.g., I-beam), or no free edges (e.g., a tube).²⁶ In either case, flexural elastic constants, especially in the axial load direction, are of primary importance. At present, relations among crippling stresses, compressive stresses, and incipient buckling must be found empirically. The buckling failure mode in composites may also be influenced by the ply-stacking sequence. Delaminations or flaws can be expected to affect critical buckling stresses differently if they occur in 0-degree or in 90-degree plies. This, however, is more a structural design than a materials consideration.

7. TEMPORAL STABILITY

Temporal stability is the change of dimension with time under constant temperature and minimal stress levels. Creep is possible with this definition, and in practice, effects of gravity, residual stresses, long-term viscoelastic recovery, slow phase transformations, anisotropy, or inhomogeneity may not always be separated out by measurements. In general, stability depends on fabrication sequence (residual stress relaxation). Materials with high values of MYS , E , or a high degree of isotropy or both, however, show higher temporal stability. Mirror figure changes with time have generally been small: $\sim \lambda/30 - \lambda/40$ for CER-VIT and silica mirrors.²⁷ Zerodur and Super Invar exhibit the most temporal stability,^{28,29} but a single figure of merit based on material properties cannot yet be defined. Jacobs²⁹ suggested a coefficient of temporal expansion (CtE) or α_t equal to $\Delta L/L\Delta t$ and analogous to $CtE \alpha_T$. Covalent bonding and low dislocation densities promote good temporal stability. Silicon and silicon carbon should be quite stable on this basis. Birefringence is useful for measuring residual stresses in glasses or

other transparent materials, but comparable tests do not exist for opaque mirror substrates, with the possible exception of x-ray methods.

Residual stresses often result in cracking, which results in distortion. They need not exceed the ultimate tensile stress to cause mirror degradation. Stresses may open already existent cracks or enhance interfacial strains near imperfections or at coating substrate interfaces. Cracks may originate from grinding, stress waves, and vibrational modes, which enhance microstructural stress risers. They are influenced by variations in CTE, composition, porosity, inclusions, crystal orientation, residual stresses that result from thermomechanical treatments, and pre-existing microcracks. A theory for handling macroscopically homogeneous isotropic materials that contain randomly oriented cracks has been developed at Aerospace.³⁰ These results can be incorporated into a finite element code that can be used to predict the failure probability of a structure subject to arbitrary stresses. Material parameters include fracture stress, which is roughly proportional to $(2\gamma Ed^{-1})^{1/2}$ where γ is the surface energy of a crack and d is the interatomic spacing. While cracking will usually result in a net dimensional change (and mirror distortion), surface cracking also has significant effects on β , which then causes increased and possibly excessive thermal effects. Cracks that open in the mirror surface may affect the radius of curvature, but the nature of the stress state relieved will also determine the magnitude of the resultant deformation δ . Extreme hardness, usually found with cohesively bonded atomic structures, promotes the ability to grind to a high level of surface perfection. When the surface can be ground to $\lambda/100$ or better, radiation or EMP surface damage thresholds approach the bulk values. Voids are undesirable. Another consideration in grinding is the number of support points N required to achieve a given level of surface perfection χ . For $\lambda/20$, $\chi \sim 0.025\mu\text{m}$:³¹

$$N = \frac{1.5a^2}{h} \sqrt{\frac{\rho}{E\chi}} \quad (18)$$

This suggests that E/ρ should be maximum for effective grinding and polishing of the mirror.

8. COATING EFFECTS

Coatings are chosen for different material properties than the mirror substrate. These include spectral reflectivity, damage tolerance, adhesion, dielectric properties, refractive indices, and abrasion resistance. Anticipation of actuators and deformable mirror substrates requires special attention to reflective coatings and substrate adhesion during thermal cycling. Rowe demonstrated that while cracking or even appreciable reflectance variation may not occur, small changes in absorptance are found.² Damage thresholds are likely to be different than the substrate. They also depend on the mode of fabrication; evaporated gold, for example, has a lower laser damage threshold than plated gold.³²

Thermal-expansion mismatches induce surface stresses in the substrate. These may be estimated³³ for a coating-substrate-coating sandwich,

$$\sigma(\text{substrate}) = EAT(\alpha_s - \alpha_c) j(1 - 3j + 6j^2) \quad (19)$$

The ΔT may refer to the thermal excursion seen, or the temperatures involved in the application of the coatings. If microcracking does not relieve these stresses, microdeformation of the substrate may result, especially if $\sigma > \text{MYS}$.

B. THERMAL-LOADING EFFECTS

Three categories of effects are considered here: 1) steady-state heating deflections, 2) transient deflections, and 3) surface damage.

1. STEADY-STATE DEFLECTIONS

Separate distortions occur 1) if the rear surface is kept in radiative contact with a heat sink, 2) when uniform temperature excursions occur, and 3) when linear gradients arise, depending on the curvature of the mirror. These six distortions are described in subsections B.1.a through B.1.f.

a. $T_b = T_o$, Curved Mirror

The back-face temperature T_b is assumed to be equal to that of a backup structure T_o because of radiative coupling. It is also assumed that there is no reradiation from the front face. The surface deflection is then¹

$$\delta = \frac{-a^2 \alpha_{11}}{2R} (\beta Q) \left[\frac{m}{2k_1 \rho} + \frac{1}{4\alpha_B T_o^3 F_e} \right] \quad (20)$$

The predominant material parameter is K_1/α_{11} , since $m/\rho = h$. To compare materials on this basis, constant h and m must be assumed, and the fact that k and α may vary with T must be considered. In addition, very porous materials will benefit by being considered as foil-foam-foil sandwiches.

b. $T_b = T_o$, Flat Mirror

In this case, $R \rightarrow \infty$, so that δ in Eq. (20) approaches zero.

c. $\Delta T_b = \Delta T_s$, Curved Mirror

For a uniform thermal change, e.g., to operating temperature,

$$\delta = \frac{a^2}{2R} \bar{\alpha}_{11}(T) \Delta T_u \quad (21)$$

the change in radius of curvature is $R \alpha_{11} \Delta T_u^3$.

d. $\Delta T_b = \Delta T_s$, Flat Mirror

The deflection of Eq. (21) goes to zero as $R \rightarrow \infty$. However, an out-of-plane growth for a flat plate, which is given by

$$\delta = \frac{m}{\rho} \bar{\alpha}_1(T) \Delta T_u \quad (22)$$

can be considered. This is generally assumed to be correctable by actuators when ΔT_u has been achieved or by initial focusing.

e. $T_s \rightarrow T_b$ Linearly, Flat Mirror

For a circular mirror,

$$\delta = \frac{-a^2}{2} \frac{\alpha_{11}}{k_1} (\beta Q) = \frac{-a^2}{2} \frac{\alpha \Delta T}{h} \quad (23)$$

since $\beta Q = k\Delta T/h$ for steady-state heat flow. If T_s is high, the flux is re-radiated and the effective β is not constant. A similar expression has been derived for a rectangular mirror of sides a and b ³⁴

$$\delta = \left(\frac{a^2 + b^2}{8} \right) \frac{\alpha}{k} (\beta Q) = \frac{a^2 + b^2}{8h} \alpha \Delta T \quad (24)$$

f. $T_s \rightarrow T_b$ Linearly, Curved Mirror

Equations (23) and (24) apply also in this case.

g. Variations in CTE

The preceding subsections indicate α_{11} and α_1 are important. There may be local variations in either of these, so that

$$\delta = \frac{3}{4} \frac{a^2 \rho}{m} \Delta \bar{\alpha}_{11} \Delta T_u \quad (25)$$

which is derived in Ref. 1 on the basis of equal layers with different $\bar{\alpha}_{11}$ values ($\Delta \bar{\alpha}_{11} = \bar{\alpha}_1 - \bar{\alpha}_2$). This is also equivalent to a change in R . Localized bumps occur as a result of variation in $\bar{\alpha}_1$ while traveling along the surface, so an equation in Ref. 35 is also applicable.

$$\delta = h\Delta\bar{\alpha}_1\Delta T \quad (26)$$

which is equivalent to local variations in out-of-plane growth.

Another approach to the effect of local α gradients is to consider non-uniform (e.g., Gaussian) incident irradiation. The local distortion given by Ref. 36 is:

$$\delta(r) = - \frac{(1 + \nu) \alpha \beta Q w^2}{2\rho C_p} \int_0^\infty e^{\left(\frac{-\zeta^2 w^2}{8}\right)} J_0(\zeta r) \{T\} \zeta d\zeta \quad (27)$$

where the $\{T\}$ term contains mainly transient equilibration terms. Local deformation $\delta(r,t)$ then depends on $(1 + \nu)\Delta\alpha/\rho C_p$, and variations in surface figure with time are also affected by variations in α . In this case, the model assumes isotropic properties, so that transverse effects of $\Delta\alpha_{11}$ vs $\Delta\alpha_{11}$ require further investigation. This analysis indicates that variations in α may be variations in β , ρ , C_p , and k , all of which affect the transient surface figure. Nevertheless, α is the predominant material parameter for thermal effects.

2. TRANSIENT DEFLECTIONS

All thermal deformation or damage modes are time dependent; it is of interest to investigate the material parameters that control the time required to reach a failure mode or to equilibrate to a constant deflection. A convenient approach to transient effects is suggested by the work of Sparks.⁸

For short times, that is $t < \rho C_p h^2/3k$,

$$\beta(T)Q = \sqrt{\pi\rho C_p k} (1/t)^{1/2} (T - T_0) \quad (28)$$

This implies that a temperature-dependent heat flux (with a beam diameter that greatly exceeds the mirror thickness) is equal to the product of a material parameter, an applicable time interval, and a failure criterion expressed as an unacceptable temperature rise. For example, $T - T_0$ may be the interval required to cause melting ($T_m - T_0$), excessive thermally induced stresses, or fracture. Equation (28) indicates that for a given time, ΔT of the surface is minimized if $k\rho C_p$ is maximized. This time region applies to the initial interval where damage or distortions occur before correction, by such methods as actuators or active cooling, can be effective. A useful approximation for $\beta(T)$ is $\beta_0 (\Delta T/T_0)^{1/2}$. Another expression uses the threshold intensity I_D ^{31,32}

$$\beta I_D = (T_m - T_0) \sqrt{k\rho C_p} \quad (29)$$

where T_m refers to the lowest melting point in the coating-substrate system. This equation applies fairly well unless there is poor adherence of the surface films. Monsler³⁸ defines a fluence limit, a maximum energy per pulse in terms of melt damage as:

$$J_m (\text{J/cm}^2) \sim \beta \sqrt{\tau_p} \sim \sqrt{\tau_p/\lambda} \quad (30)$$

The maximum intensity allowed is then

$$I_{\max} = J_m / \tau_p \sim (\tau_p)^{1/2} \quad (31)$$

In longer pulse times, dirt particles can explode and form an absorbing plasma of material, which can transfer absorbed radiation to the surface by electronic heat conduction. Then⁸

$$I_m \sim \lambda^{-2} \tau_p^{-1} \quad (32)$$

Vaporization damage is described³⁷ by the rate of the inward vapor-liquid boundary movement. To minimize the surface figure change, ρL_e should be maximized. Additional discussions of melting and vaporization damage mechanisms, which use similar mathematical models, are given in Refs. 39 through 42. The exact mechanism for incipient melting damage, for example, may be more shifting of grain boundaries (before absorption of the heat of melting). Rear surfaces of transparent materials generally have lower damage thresholds than bulk or front surfaces, because plasma created near the surface tends to absorb radiation. Back-scattered radiation or specular reflectance to measure laser damage may be effective. However, clear-cut definitions of threshold are not always available. Total reflectance may not be appreciably affected until the boiling point of the surface material is approached.⁴²

For longer times, $\Delta T = f(z, t)$ can be first considered.

$$T(z, t) = \frac{\beta Q h}{k} \left[\frac{kt}{\rho C_p h^2} + \frac{3z^2 - h^2}{6h^2} - \sum_{n=1}^{\infty} \frac{(-1)^n}{n^2} \exp \left(\frac{-kn^2 \pi^2 t}{\rho C_p h^2} \right) \cos \left(\frac{n\pi z}{h} \right) \right] \quad (33)$$

The thermal diffusivity $k/\rho C_p$ is an important parameter in the ability of a material to athermalize. The average temperature in the mirror, or

$$\bar{T} = \frac{1}{h} \int_0^h T(z, t) dz$$

determines the average strain, so that, analagous to Eq. (28), the surface distortion is described as:

$$\beta Q t = \left(\frac{\alpha}{\rho C_p} \right) \Delta h \quad (34)$$

which is applicable to $t > \rho C_p h^2 / 3k$.⁸ Here, the input heat energy is equated to the product of a material parameter term and a geometrical failure criterion. The distortion is independent of the thermal conductivity, whereas the surface temperature depends very much on thermal conductivity [Eq. (33)]. Similar forms of this equation are derived depending on interest in bowing or uniform growth criteria for excessive deflections. For example,

$$\beta Q t = \left(\frac{\rho C_p}{\alpha} \right) \left(\frac{\delta h^2}{2a^2} \right) \quad (35)$$

for bowing before the back face starts rising in temperature. The extent of this deflection as a function of r is given as⁵

$$\delta = \frac{6}{\sqrt{3}} \frac{(a^2 - r^2)}{h^2} \left(\frac{\alpha}{\rho C_p} \right) \beta Q t \quad (36)$$

while more uniform growth is simply experienced as^{5,35,43}

$$\delta = 2 \left(\frac{\alpha}{B \rho C_p} \right) \beta Q t \quad (37)$$

The situation is slightly more complex when Gaussian irradiance is considered, as indicated by Eq. (27). The time required for the back face to reach one-

half its ultimate temperature when exposed to a laser pulse is proportional to $\rho C_p k$.⁴⁴

3. THERMALLY INDUCED FAILURE

Melting or vaporization failure criteria are discussed in the preceding subsection. Thermal-loading effects, especially at higher flux levels, challenge the strength of the material. Permanent deformations may result if stresses exceed the microyield strength; cracking occurs if they exceed the ultimate strength. A major effect of cracking may be an increase in absorptivity.

a. Cracking Caused by Thermal Gradients

Nonuniform heating of the surface will produce local stresses, which can be estimated from the equation given by Apollonov.³⁶ For stresses that result from a Gaussian power density with beam parameter $w \ll 2a$,

$$\sigma_{rr} = -\frac{\alpha_{11} \beta Q E w^2}{4k} \int_0^\infty e^{-\left(\frac{\xi^2 w^2}{8}\right)} \frac{J_1(\xi r)}{\xi r} d\xi \quad (38)$$

$$\sigma_{\theta\theta} = -\frac{\alpha_{11} \beta Q E w^2}{4k} \int_0^\infty e^{-\left(\frac{\xi^2 w^2}{8}\right)} \left[J_0(\xi r) - \frac{J_1(\xi r)}{\xi r} \right] d\xi \quad (39)$$

These thermal stresses depend on ratios of $k/\alpha E$. These equations and Eq. (27) are used by Apollonov to designate incident power levels corresponding to successively more severe surface deformation, from elastic to plastic flow to melting. In each case, the material parameters are different:

1. Local power density to exceed elastic distortion $\sim k/\alpha(1 + \nu)$
2. Local power density to reach flow stage $\sim \text{flow stress} \times (k/\alpha E)$
3. Local power density to cause melting $\sim T_m$

b. Thermal Fatigue

If we equate the thermally induced strain ϵ to a constrained stress

$$\epsilon = \alpha \Delta T = \frac{\alpha(1 - \nu)}{E} \quad (40)$$

and insert ΔT from Eq. (28) for short-time transient effects, an expression is obtained for the thermal stress limit α :

$$\alpha = \frac{E\epsilon}{(1 - \nu)} (\beta Q t) (\pi \rho C_p k T)^{-1/2} \quad (41)$$

where α is chosen to correspond to the degree of distortion allowable, from MYS to cracking to the ultimate tensile strength. The $\beta Q t$ term is the energy per unit area and could be a pulse. Sparks⁴⁵ presents similar equations for various heating and cooling conditions.

Thermal cycling induces thermal fatigue through such mechanisms as differential expansion of inhomogeneities, thermal gradients, and thermally induced stress effects (e.g., visco-elastic recovery). Mirror samples have been measured for figure change as a result of thermal cycling.²⁴ Composites are always susceptible to microcracking; it might be desirable to minimize the spread of CTEs of the constituents and maximize the strain capability of a matrix phase.

c. General Damage Mechanisms

A general introduction to laser damage of optical components has been provided by Bass.⁴⁶ The importance of absorptivity β , surface defects, and inclusions is particularly stressed. Surface irregularities contribute to scattering and image degradation. Parameters such as rms roughness and geometrical features of the surface, although often critical in considerations of laser damage, are a function of mirror fabrication and not (immediately) of the mirror material, and so are beyond the scope of these considerations. Inclusions, however, and compositional variations are often typical of a

material. Grain size of the parent material may determine the location and size of inclusions. Hardness and polishing characteristics determine the polishing method, which in turn determines the types of imbedded particles that may be found.

Glass and Guenther² indicate the difficulty in characterizing the surface and isolating one particular feature to determine its exact role in damage phenomena. Porteus² demonstrates that stress-wave induced damage may include slip, pit, or crater production; ion and light emission; and work-function changes. Intrinsic material properties determine which damage mechanism occurs first, as well as the fabrication procedures. Peak thresholds were 15 J/cm² for slip to occur, as compared to about 40 J/cm² for melting of the same diamond-turned Cu mirror. Damage thresholds require energies of > 1 MW/mm². Diamond-turned Cu, for example, has a damage threshold of close to 10 MW/mm² (Ref. 32).

Sparks gives a useful figure of merit for the amount of cooling required to avoid excessive optical distortion for a given value of $\beta Q \tau_p$.⁴⁷

IV. FIGURES OF MERIT

Table II summarizes the major material figures of merit related to the principal causes of mirror failure. In a mirror design, the relevant geometrical parameters of loading conditions must be combined with the material parameters. Alternative figures of merit, such as maximum permissible pulse energy,⁴⁸ are derived in a straightforward manner from the preceding analysis. The figures of merit listed in Table II provide a guide to the development of new mirror materials. The k/α or $\rho C_p/\alpha$ combinations for thermal effects are strong incentives for minimizing α . Pirooz *et al.*,⁴⁹ for example, compare a near zero CTE material (Cu-doped CER-VIT) to other materials on the basis of the $\rho C_p/\alpha$ parameter. Similar considerations encouraged other zero CTE research, including Al-Nb₂O₅ studies at the Massachusetts Institute of Technology, WC coated graphite in graphite-carbon composites at General Dynamics, isotropic hot pressed mixtures of positive and negative CTE materials at Aerospace, and Li₂O-Al₂O₃-SiO₂ studies at Pennsylvania State University and Owens-Illinois.⁴⁹

Although the CTE is the single most important material parameter involved, there are eight CTEs: α_1 , α_{11} , $\bar{\alpha}_1$, $\bar{\alpha}_{11}$, $\Delta\alpha_{11}$, $\Delta\alpha_1$, $\Delta\bar{\alpha}_{11}$, and $\Delta\bar{\alpha}_1$. The latter four (distributions or variations in α) have rarely been measured and must often be inferred from limited reports of refraction, ultrasonic velocity,⁵⁰ or figure distortions by holographic interferometry. The combination of a particular α into a generalized figure of merit is difficult, since it can be absolute zero on occasion, but this does not necessarily ensure adequate mechanical properties or even other α values that are adequate.

Mechanical considerations require a high E/ρ or E/ρ^3 value and a high microyield strength. The design parameters do not, however, account very well for possible deficiencies in dimensional stability. Thermal cycling, micro-creep, and viscoelastic moisture or radiation effects, for example, require additional sets of material parameters for a full description. These include the coefficient of moisture expansion (CME), the coefficient of cracking expansion (CCE), and activation energies for creep or time-dependent recovery mechanisms. In one instance,⁵¹ the optics housing for cryogenic sensors was described by the figure of merit:

$$\frac{kE(\text{MYS})}{\rho C_p \alpha}$$

Numerically, graphite-epoxy was about seven times better than Be, but the latter material was used because of unknown microcracking tendencies of graphite-epoxy at low temperatures. These cracking effects are often eliminated by extensive low-temperature thermal cycling. However, the effects on the other dimensional stability and mechanical properties, such as moisture absorption or microyield strength, are not determined. Dimensional stability effects on composites are further reviewed in Ref. 52.

Table II indicates that material parameters such as E , k , L_e , T_m , G , and all the strength properties should be maximum, while all α 's should be minimum. The mechanism involved determines whether C_p , ρ , and ν should be maximum or minimum. For mechanical loads, ρ should be minimum, but for removal of temperature gradients and minimized laser damage, a larger density is desirable. To minimize thermally induced distortions C_p should be high, but it should be low to provide rapid equilibration (a high thermal diffusivity). Transient uniformly irradiated distortions are governed by $\alpha/\rho C_p$, but temperature changes, flux gradients, and laser damage depend on $(k/\rho C_p)$. Variations in C_p and ν are seldom more than a factor of 2 or 3 for most materials, so generalized figures of merit do not require them. The simplest generalized figure of merit would then be

$$\left(\frac{k}{\Delta\alpha + \alpha} \right) \left(\frac{E}{\rho} \right) (\sigma\Lambda\psi)$$

which should be maximized for mirror materials. A relevant strength property (e.g., MYS or UTS) is represented by σ , Λ is a thermal criterion such as $T_m L_e$, and ψ is a dimensional stability parameter such as the CME^{-1} or CCE^{-1} . The problem of an infinite figure of merit when α approaches zero is solved by adding the variation in α . The residual variability in α also relates to fabrication and polishing aspects of the mirror. Polishing characteristics would otherwise be represented by E and α , in turn related to hardness.

REFERENCES

1. F. Ayer, E. G. Wolff, and G. G. Comisar, "Materials for Large Space Optics," 1977 International Thermal Expansion Symposium, Manitoba, Canada, 29-31 August 1977; also, Thermal Expansion 6, I. D. Peggs, ed., Plenum Press, New York (1978), pp. 27-41.
2. A. Glass and A. H. Guenther, "A Decade of Damage--Report on 10th Annual Symposium on Optical Materials for High Power Lasers," Electro. Opt. Syst. Des., 35-39 (April 1979). See also report on 9th Symposium, Appl. Opt. 17 (15), 2386 (1978).
3. E. A. Sziklas et al., System Optical Quality Study, Phase I--Problem Definition, AFWL-TR-73-231, AD920867, Pratt and Whitney Aircraft, West Palm Beach, Florida (June 1974).
4. M. Born and E. Wolf, Principles of Optics, Second (Revised) Ed., MacMillan, New York (1964).
5. H. E. Bennett, "Thermal Distortion Thresholds for Optical Trains Handling High Pulse Powers," Laser Induced Damage in Optical Materials: 1976, NBS Special Publication 462 ASTM-STP-622, A. J. Glass and A. H. Guenther, ed. (Dec. 1976), pp. 11-24; Proc. ASTM Symposium, Boulder, Colorado, July 13-15, 1976.
6. H. V. Winsor, "Basic Properties of High Power/Quality Beam Trains," Conference on High Power Laser Windows, Vol. III., C. A. Pitha, ed. AFCRL-TR-74-0085, Vol. III (12-14 Nov. 1973).
7. M. H. Krim, "Design of Highly Stable Optical Support Structure," Opt. Eng. 14 (6), 552-558 (1975).
8. M. Sparks, "Theory of Laser Heating of Solids: Metals," J. Appl. Phys. 47 (3), 837-849 (Mar. 1976).
9. M. Sparks, "Optical Distortion by Heated Windows in High Power Laser Systems," J. Appl. Phys. 42 (12), 5029-5046 (Nov. 1971).
10. W. B. Elmer, The Optical Design of Reflectors, W. B. E., Andover, Mass. (1974).
11. A. J. Malvick, "Thermal Deformations of Solid Mirrors," Appl. Opt. 9 (11), 2481-2484 (1970). See reports under Project THEMIS (AFOSR) - Thermal Distributions of Mirrors (1970).
12. J. P. Duncan, "Self-Weight Loaded Structures in the Context of Lightweight Mirror Applications," Opt. Telescope. Tech., NASA-SP-233 (1970), pp. 251-270.

13. C. M. Percival "Laser-Generated Stress Waves in a Dispersive Elastic Rod," J. Appl. Phys. 38 (13), 5313-5315 (Dec. 1967).
14. R. D. Carnahan, "Microplasticity, Its Measurement and Application to Guidance and Control Components," J. Met. 16, 990-994 (Dec. 1964).
15. H. R. Garcia and L. D. Brooks, "Characterization Techniques for Deformable Metal Mirrors," Proc. Soc. Photo. Opt. Instrum. Eng. 141, 74-81 (March 1978).
16. W. E. Howell, "Recent Advances in Optical Control for Large Space Telescopes," Space Optics, B. J. Thompson and R. R. Shannon, ed., National Academy of Science (March 1975), pp. 239-258.
17. R. M. Scott, "New Technique for Controlling Mirror Shapes," Opt. Eng. 14 (2), 112-115 (March 1975).
18. C. B. Hogge, "Optical Distortion in High Energy Laser Systems Active Control," Proc. Soc. Photo. Opt. Instrum. Eng., 140-145 (1977).
19. W. Lee Smith, "Laser-Induced Breakdown in Optical Materials," Opt. Eng. 17 (5), 489-503 (1978).
20. J. E. Pearson and S. Hansen, "Experimental Studies of a Deformable - Mirror Adaptive Optical System," J. Opt. Soc. Am. 67 (3), 325-333 (1977).
21. N. T. Adelman, "Spherical Mirror with Piezoelectrically Controlled Curvature," Appl. Opt. 16 (2), 3075-3077 (1977).
22. W. P. Barnes, "Transverse Deflections of a 45 inch Diameter, Lightweight Mirror Blank: Experiment and Theory," Optical Telescope Technology, NASA-SP-233 (1970), pp. 287-290; also, Appl. Opt. 8, 1191 (1969).
23. L. A. Selke, "Theoretical Elastic Deformations of Solid and Cored Horizontal Circular Mirrors having a Central Hole on a Ring Support," Appl. Opt. 10 (4), 939-944 (1971).
24. C. W. Marschall and R. E. Maringer, Dimensional Stability - An Introduction, Pergamon Press (1977).
25. L. B. Greszczuk, "Compressive Strength and Failure Modes of Unidirectional Composites," ASTM-STP-521 (1973), pp. 192-217.
26. E. E. Spier, "Stability of Graphite/Epoxy Structures with Arbitrary Symmetrical Laminates," Exp. Mech. 18, 401-408 (Nov. 1978).

27. J. M. Jerke and R. J. Platt, Dimensional Stability Studies of Candidate Space-Telescope Mirror Substrate Materials, NASA-TN-D6626 (Jan. 1972).
28. F. Rehn and V. O. Jones, "Vacuum Ultraviolet and Soft X-ray Mirrors for Synchrotron Radiation," Opt. Eng. 17 (5), 504-511 (1978).
29. S. F. Jacobs, "Measurements of Ultrasmall Displacements," Opt. Eng. 17 (5), 544-546 (1978).
30. S. B. Batdorf, "A Statistical Theory for Failure of Brittle Materials Under Combined Stresses," AIAA Paper No. 73-381, 14th Structures Conference, Virginia, March 1973.
31. H. D. Hall, Problems in Adopting Small Mirror Fabrication Techniques to Large Mirrors, NASA-SP-233 (1970), pp. 149-152.
32. R. Gibbs and R. M. Wood, Laser-Induced Damage of Mirror and Window Materials at 10.6 μ m, NBS Special Publication 462 (1976), pp. 181-187 (See Ref. 5)
33. W. D. Kingery, Introduction to Ceramics, Wiley & Sons, New York (1960).
34. E. G. Wolff and S. A. Eselon, "Thermal Expansion of a Fused Quartz Tube in a Dimensional Stability Test Facility," Rev. Sci. Instrum. 50 (4), 502 (1979).
35. R. C. McNamara et al., Materials for Large Space Optics, Phase I Final Technical Report CASD-AFS-77-008 Contract F33615-77-C-5247, General Dynamics, Convair Division City (January 1978).
36. V. V. Apollonov, A. I. Barchukov, and A. M. Prokhorov, "Optical Distortion of Heated Mirrors in CO₂-Laser Systems," IEEE J. Quantum Electron. QE-10 (6), 505-508 (June 1974).
37. J. F. Ready, "Effects Due to Absorption of Laser Radiation," J. Appl. Phys. 36 (2), 462-468 (Feb. 1965).
38. M. Monsler, "High Power Optics," Opt. Eng. 15 (2), 158-165 (March-April 1976).
39. W. J. Spawr and R. L. Pierce, Metal Mirror Selection Guide, SOR Report No. 74-004, Spawr Optical Research Inc., Corona, California (May 1976).
40. V. V. Apollonov et al., "Cooled Laser Mirror," Kvant. Elektron 5 (5), 1169; also, Laser Focus, 14 (8), 98 (Aug. 1978).
41. C. R. Guiliano, Laser Induced Damage in Optical Materials, AFCRL-TR-73-0528, Hughes Research Laboratories, Malibu, California (July 1973), and AFCRL-TR-0104 (Feb. 74).

42. K. Park and W. T. Walter, "Metal Reflectance Changes during Intense Irradiation," ASM Conference on Applications of Lasers in Materials Processing, 18-20 April 1979.
43. J. S. Accetta and R. F. Shea, "Sources of Optical Distortions in High Energy Laser Systems," Proc. Soc. Photo. Opt. Instrum. Eng. 121, 132-139 (Aug. 1977).
44. M. Kuriyama et al., "Thermal Conductivity of Hot Pressed Si_3N_4 by the Laser Flash Method," Ceram. Bull. 57 (12), 1119-1122 (1978).
45. M. Sparks, "Stress and Temperature Analysis of Surface Cooling or Heating of Laser Window Materials," J. Appl. Phys. 44 (9), 4137 (1973).
46. M. Bass, "Mechanisms of Laser Damage to Optical Components," Proc. Soc. Photo. Opt. Instrum. Eng. 121, 6-10 (1977).
47. M. Sparks and C. J. Duthler, "Theoretical Studies of High Power Ultraviolet and Infrared Materials," 8th Technical Report, DAAC-15-73-C-0127 (DARPA) Xonics, Santa Monica, California (31 Dec. 1976).
48. H. Winston and G. S. Picus, Universal Curves for Window Material Figures of Merit, "AFCRL-TR-0085 Vol. III, Hughes Research Laboratories, Malibu, California (1973), p. 1099.
49. P. P. Perooz and G. Duke, Generation of Copper Films on Low-Expansion Substrates for Use as Laser Mirrors, Report AFML-TR-78-139, Owens-Illinois (Oct. 1978).
50. H. E. Hagy and W. D. Shirkey, "Determining Absolute Thermal Expansion of Titania-Silica Glasses: A Refined Ultrasonic Method," Appl. Opt. 14 (9), 2099-2103 (1975).
51. J. M. Miller, "Computer-Aided Design and Evaluation on Infrared Cryogenic Sensors Undergoing Thermal/Mechanical Distortion," Proc. Soc. Photo. Opt. Instrum. Eng. (1978); also, Vol. 121 pp. 146-155 (1977).
52. E. G. Wolff, "Dimensional Stability of Structural Composites for Spacecraft Applications," Met. Prog. 115 (6), 54-63 (1979).
53. J. W. Berthold III, S. F. Jacobs, and M. A. Norton, "Dimensional Stability of Fused Silica, Invar, and Several Ultralow Thermal Expansion Materials," Appl. Opt. 15 (8), 1898-1899 (Aug. 1976).
54. W. A. Eul and W. W. Woods, Effects of Surface Polishing on the Microstrain Behavior of Telescope Mirror Materials, "NASA-CR-112217, Boeing Aerospace Co., Seattle, Washington.

55. F. F. Forbes and H. L. Johnson, "Stability of Tenzaloy Aluminum Mirrors," Appl. Opt. 10 (6), 1412 (1971).
56. J. B. Schroeder, "Materials Considerations for Large Spacebourne Astronomical Telescopes," Optical Telescope Technology, NASA-SP-233 (1970), pp. 141-148.
57. A. J. Glass and A. H. Guenther, "Laser Induced Damage in Optical Materials: 8th ASTM Symposium," Appl. Opt. 16 (5), 1214-1231 (May 1977).
58. V. Wang, A. I. Braunstein, and J. Y. Wada, "Investigation of Pulsed CO₂ Laser Damage of Metal and Dielectric-Coated Mirrors," NBS Special Publication 371, Proc. ASTM Symposium on Laser Induced Damage, June 14-15, 1972 (October 1972), pp. 183-193.
59. J. M. Miller, "Thermal Deformation Characteristics of a Six-Inch Graphite/Epoxy and Ultra-Low-Expansion Mirror Telescope," J. Spacecraft Rockets 14 (5), 315 (May 1977).
60. A. H. Clauer, "Interactions of Laser Induced Stress Waves with Metals," Proc. of ASM Conference on Applications of Lasers in Materials Processing (April 1979), pp.18-20.

SYMBOLS

a	radius of circular mirror dish
D	flexural rigidity = $Eh^3/12(1 - \nu^2)$
C_p	specific heat (w-s/Kg-K)
d	height of I beam support
E	elastic (Young's) modulus
F	amplitude of dynamic disturbance
F_e	radiation coupling factor
G	shear modulus
g	earth gravitation acceleration (9.81 m-s^2)
h	thickness of mirror substrate = m/ρ
I	far-field intensity; moment of inertia
J_0	zero-order Bezel function
j	ratio of coating to substrate thickness
k	thermal conductivity ($\text{W-m}^{-1}\text{-k}^{-1}$)
L	length
l	distortion or length
L_e	heat of melting
MYS	microyield strength
m	mass per unit area = h^{*****}
N	number of support points for mirror
p	distributed load
Q	incident heat flux or irradiance (W-m^{-2})
R	radius of curvature of mirror
r	radial in-plane coordinate
r_G	radius of gyration
u	displacement coordinate
UTS	ultimate tensile strength
w	localized beam parameter
x	in-plane mirror coordinate
y	in-plane mirror coordinate
z	thickness direction coordinate

Greek Symbols

α	coefficient of thermal expansion ($^{\circ}\text{K}^{-1}$)
β	absorptivity, also coefficient of moisture expansion ($\% \text{M}^{-1}$)
γ	coefficient of cracking expansion (CCE)
δ	central deflection of mirror
ϵ	strain or $\Delta L/L$
ζ	bessel function parameter in Eq. (27)
η	geometrical ratio [see Eq. (17)]
θ	radial in-plane coordinate of mirror plane
λ	wavelength
μ	micro
ν	Poisson's ratio
ξ	damping ratio of mirror assembly
ρ	aperture radius, material density
σ	figuring error, stress
τ	pulse time
ϕ	phase aberration (rad)
χ	surface perfection
ψ	selected dimensional stability parameter
ω	2π frequency
Δ	change in
Λ	selected thermal-damage parameter
σ_{β}	stefan-Boltzmann constant

Subscripts

b	back face
c	compressive
i	perpendicular to incident flux
ll	parallel to mirror plane
o	initial or operating; back-up structure
rms	root mean square

Subscripts (Continued)

s	solid (rectangular cross section), front surface
cr	critical
e	latent, also used in radiation coupling factor (F_e)
m	maximum or melting (for T_m)
p	pulse
f	figure (error)
u	uniform

LABORATORY OPERATIONS

The Laboratory Operations of The Aerospace Corporation is conducting experimental and theoretical investigations necessary for the evaluation and application of scientific advances to new military concepts and systems. Versatility and flexibility have been developed to a high degree by the laboratory personnel in dealing with the many problems encountered in the nation's rapidly developing space and missile systems. Expertise in the latest scientific developments is vital to the accomplishment of tasks related to these problems. The laboratories that contribute to this research are:

Aerophysics Laboratory: Launch and reentry aerodynamics, heat transfer, reentry physics, chemical kinetics, structural mechanics, flight dynamics, atmospheric pollution, and high-power gas lasers.

Chemistry and Physics Laboratory: Atmospheric reactions and atmospheric optics, chemical reactions in polluted atmospheres, chemical reactions of excited species in rocket plumes, chemical thermodynamics, plasma and laser-induced reactions, laser chemistry, propulsion chemistry, space vacuum and radiation effects on materials, lubrication and surface phenomena, photo-sensitive materials and sensors, high precision laser ranging, and the application of physics and chemistry to problems of law enforcement and biomedicine.

Electronics Research Laboratory: Electromagnetic theory, devices, and propagation phenomena, including plasma electromagnetics; quantum electronics, lasers, and electro-optics; communication sciences, applied electronics, semiconducting, superconducting, and crystal device physics, optical and acoustical imaging; atmospheric pollution; millimeter wave and far-infrared technology.

Materials Sciences Laboratory: Development of new materials; metal matrix composites and new forms of carbon; test and evaluation of graphite and ceramics in reentry; spacecraft materials and electronic components in nuclear weapons environment; application of fracture mechanics to stress corrosion and fatigue-induced fractures in structural metals.

Space Sciences Laboratory: Atmospheric and ionospheric physics, radiation from the atmosphere, density and composition of the atmosphere, aurorae and airglow; magnetospheric physics, cosmic rays, generation and propagation of plasma waves in the magnetosphere; solar physics, studies of solar magnetic fields; space astronomy, x-ray astronomy; the effects of nuclear explosions, magnetic storms, and solar activity on the earth's atmosphere, ionosphere, and magnetosphere; the effects of optical, electromagnetic, and particulate radiations in space on space systems.

THE AEROSPACE CORPORATION
El Segundo, California